How the laser beam size conditions the temporal contrast in pulse stretchers of CPA lasers

Simon Roeder[1,2,*], Yannik Zobus[1,2], Christian Brabetz[1], and Vincent Bagnoud[1,2,3]

[1]*GSI Helmholtzzentrum für Schwerionenforschung GmbH, Darmstadt, Germany*
[2]*Technische Universität Darmstadt, Darmstadt, Germany*
[3]*Helmholtz-Institut Jena, Jena, Germany*
[*]*Corresponding author: s.roeder@gsi.de*

Abstract
In this work, we propose and verify experimentally a model that describes the concomitant influence of the beam size and optical roughness on the temporal contrast of optical pulses passing through a pulse stretcher in CPA laser systems. We develop an analytical model that is capable of predicting the rising edge caused by the reflection from an optical element in a pulse stretcher, based on the power spectral density of the surface and the spatial beam profile on the surface. In an experimental campaign, we characterize the temporal contrast of a laser pulse that passed through either a folded and an unfolded stretcher design and compare these results to the analytical model. By varying the beam size for both setups, we verify that optical elements in the near- and the far-field act opposed to each with respect to the temporal contrast and that the rising edge caused by a surface benefits from a larger spatial beam size on that surface.

Keywords: CPA Laser, Temporal Contrast, Stretcher

1. Introduction

The temporal profile of short laser pulses generated by high-intensity lasers exhibit complex features commonly referred to as "temporal contrast". The issue of temporal contrast degradation has been studied ever since the invention of the chirped-pulse amplification (CPA) technique[1] because of its deleterious effect on high-intensity-laser-driven experiments. Temporal contrast mitigation methods palliating the problem[2] were first proposed but these systematically increase the complexity of the laser architecture by adding pulse-cleaning stages, either in the front-end of the laser[3–5] or after the pulse compressor at the back-end of the laser[6–9]. Alternatively, temporal-pedestal-free amplifiers[10] can be designed to replace the first stage of amplification in CPA lasers to keep the temporal contrast in check without adding complexity to the system[11]. As a consequence, the temporal contrast becomes less and less limited by pedestals on the ns-scale and prepulses. Instead the temporal contrast is now mainly limited by a slow rising edge on the ps-scale that can be observed systematically at laser facilities all around the world[12–16]. While the effect of the slow rising edge is not as stringent as that of the nanosecond pedestal, it is still a major problem for laser-plasma interaction experiments, as the interaction of such a profile with targets remains hard to predict and it is thus a large source of uncertainty.

During the past two decades, it has been established that this slow rising edge is caused by scattering effects, which are introduced whenever a spectrally-dispersed laser pulse is reflected from a surface, such as in the stretcher and the compressor of CPA laser systems. A first indication that surface defects in the pulse stretcher map onto the residual spectral phase and influence the pulse profile was given more than 20 years ago[17]. It took over a decade after the first description of the pulse distortion before a theoretical analysis was provided[18], that generalized this effect to all spatial frequencies of stretcher optics. This for the first time, utilized the quantification of the surface imperfections that the Fourier decomposition of the surface height distribution, called the power spectral density (PSD) of the relevant surface provides. Even though it is not explicitly stated in the paper, this implies that each such reflection contributes to the rising edge and that the magnitude of it depends on the PSD of the surface. This description still neglected the spatial extension of the beam and assumed the beam to be an one-dimensional line during the propagation throughout the stretcher. Experiments verified this and showed that either the gratings[19] or optics[12] could dominate the temporal contrast degradation, in a specific setup. In both cases, optical elements of lower scattering and better quality proved to

have a beneficial effect on the temporal contrast, increasing it by one to 3 orders of magnitude.

The incorporation of the beam size into the analytical description was provided by Bromage *et al.*[20], who focused on spatio-temporal coupling effects due to surface scattering. This model, which neglected diffraction, is adapted to describe large beam sizes like in a pulse compressor. Based on this approach, the authors even proposed an experimental stretcher setup that would prove this theory[21]. Even though we are not aware that they ever followed up on the experimental verification, the theoretical work provided the means to repeat the previously made statement that two optical elements with identical PSD will produce the same rising edge, and expend on this by recognizing that for identical PSD of the surface, the reflection with the smaller beam size will introduce the larger rising edge.

In a recent work by our group[22], we corroborated the concomitant relation between beam size and stretcher optics defects in phase and amplitude on the temporal contrast, using a two-dimensional self-made ray tracing model that includes diffraction effects. One result indicated that the folding mirror commonly found in the Fourier plane of the stretcher might dominate the rising edge due to the small beam size at this location. A clear implication of this is that the temporal contrast can be improved by increasing the surface quality of this optical element[12] or even completely removing this optical element from the stretcher design, as recently demonstrated by Lu *et al.*[23,24].

In this work, we propose and validate experimentally a new analytical description of the temporal-contrast degradation based on the beam size and PSD of optical surfaces in a pulse stretcher. Furthermore, we propose to use the beam size as a new method of optical temporal-contrast control that, in comparison to Hooker *et al.* and Ranc *et al.*[12,19], does not only influence the offset of the rising edge, but can be used to manipulate the steepness of the rising edge.

In the first part, we discuss the analytical derivation of the relationship between beam size, PSD and rising edge. Our model differs from previous approaches found in the literature [18,20] because we consider that beam diffraction and propagation effects throughout the laser amplifier introduce a spatial averaging effect that must be accounted for. Afterwards we discuss the experimental stretcher setup that we used for this proof-of-principle and compare the results to the predictions that can be made using the analytical description. In the last part, we discuss the implications of this for future stretcher designs.

2. Theory

As stated above, the effect that causes the rising edge in the pulse profile is the coherent scattering introduced by a disturbed surface acting on a spectrally-dispersed laser beam. The spectral dispersion on a surface can be approximated by a linear dependency between the position on the surface and the corresponding angular frequency ω of the pulse. Since we want to include spatial averaging effects, we assume each angular frequency to share the same spatial profile $f(x)$. In addition, we suppose that the position of each wavelength on the optical element surface x_0 follows a linear dependency with the angular frequency of the spectrum, such that $x_0 = a_\omega \omega$, where the scaling factor a_ω depends on the stretcher parameters, such as the incident angle and the grating constant. It is important to note that the linear approximation is not only valid for stretcher setups with narrow bandwidths, but also for broader bandwidths, e.g. Nd:Glass systems and Ti:Sa systems. This is due to the fact that the desired length of the stretched pulse is of the same order of magnitude in most CPA systems, meaning that the size of the spectrally-dispersed beam on the optical elements in the stretcher is comparable. When this is realized by adjusting the incidence angle and the grating constant in the stretcher, the opening angle after the first grating stays roughly the same when the bandwidth increases, which dictates the accuracy of the linearization.

In order to find an analytical description of the temporal profile, we will start with a general electrical field of a short laser pulse propagating in a stretcher that can be formulated in the spectral domain as:

$$E(\omega) = E_0(\omega) e^{i\delta\phi(\omega)}, \tag{1}$$

where $E_0(\omega)$ is the undisturbed spectral field and the spectral phase introduced by the reflection from a rough surface H is given by

$$\delta\phi(\omega) = 4\pi/\lambda_0 \cdot H(\omega), \tag{2}$$

calculated from the path difference, using the simplification that the wavelength is approximately the central wavelength $\lambda \approx \lambda_0$. If we now want to expand this by a spatial dimension, we need to consider phase-averaging effects, which will be included via an integral over the spatial dimension and the spatial profile $f(x)$. This integral accounts for the beam diffraction and propagation effects throughout the laser chain, which was mentioned earlier. For simplicity we normalize the integral over this spatial profile to unity and restricted the calculation to only include one dimensional averaging in the direction of the beam dispersion, meaning that we neglect the spatial size of the beam that is not in the direction in which the grating disperses the beam. Due to the finite acceptance angle in the stretcher, we will neglect the impact of the direction that lies perpendicular to the spatial dispersion. Given these assumptions, the spectral field follows then the following integral:

$$E(\omega) = \int f(x - a_\omega \omega) e^{i\delta\phi(x)} dx E_0(\omega). \tag{3}$$

Assuming that the disturbance $\delta\phi$ is small compared to unity, the previous equation can be linearized

$$E(\omega) = \int f(x - a_\omega\omega)(1 + i\delta\phi(x))dx E_0(\omega) \quad (4)$$

$$= E_0(\omega) + i\int f(x - a_\omega\omega)\delta\phi(x)dx E_0(\omega), \quad (5)$$

where we used the normalization of the spatial profile $f(x)$ in order to execute the spatial integral for the first term. This linearization treats the scattering in a perturbative manner. The model can be extended to several surfaces, as these will just add up in the sum. Supposing that stretcher, compressor and dispersion compensate each other perfectly in the CPA system, the resulting pulse will only depend on the perturbation. The spectral field is coupled to the temporal field via Fourier transform

$$\tilde{E}(t) = \tilde{E}_0(t) + \quad (6)$$

$$i\left[\int\int e^{i\omega t} f(x - a_\omega\omega)\delta\phi(x)d\omega dx\right] \circledast \tilde{E}_0(t), \quad (7)$$

where the Fourier transform was abbreviated with the notation $\tilde{E}(t) = \mathcal{F}[E(\omega)]$ and $\circledast$ denotes a convolution product. The double integral can be separated using the substitution $x' = x - a_\omega\omega$:

$$\tilde{E}(t) = \tilde{E}_0(t) + \quad (8)$$

$$\left[\int e^{-i\frac{x'}{a_\omega}t} f(x')\frac{dx'}{-a_\omega}\int e^{i\frac{x}{a_\omega}t}\delta\phi(x)dx\right] \circledast \tilde{E}_0(t). \quad (9)$$

This can be interpreted as the (inverse) Fourier transform from the spatial domain into the spatial frequency domain at the spatial frequency t/a_ω. The spatial coordinates are therefore mapped onto the temporal coordinates via the spatial-dispersion coefficient a_ω

$$E(t) = \tilde{E}_0(t) - \frac{i}{a_\omega}\left[\tilde{f}(t/a_\omega)\tilde{\delta\phi}(t/a_\omega)\right] \circledast \tilde{E}_0(t). \quad (10)$$

If we now take the absolute square of this we get the temporal profile of the laser pulse

$$I(t) = I_0(t) + \frac{1}{a_\omega^2}\left|\left(\tilde{f}(t/a_\omega)\tilde{\delta\phi}(t/a_\omega)\right) \circledast \tilde{E}_0(t)\right|^2 \quad (11)$$

$$- \frac{2}{a_\omega}\mathbf{Im}\left(\tilde{E}_0(t)\left[\left(\tilde{f}^*(t/a_\omega)\tilde{\delta\phi}^*(t/a_\omega)\right) \circledast \tilde{E}_0^*(t)\right]\right). \quad (12)$$

Since the imaginary part is multiplied with the Fourier transform of the spectral field $\tilde{E}_0$, it is close to zero for all relevant times (significant larger than the Fourier transform limited pulse length) and can be neglected, simplifying the temporal profile to

$$I(t) = I_0(t) + \frac{1}{a_\omega^2}\left|\left(\tilde{f}(t/a_\omega)\tilde{\delta\phi}(t/a_\omega)\right) \circledast \tilde{E}_0(t)\right|^2. \quad (13)$$

If we now again assume, that the variation of $\tilde{f}\tilde{\delta\phi}$ is small over the duration of the pulse, we can simplify this even further

$$I(t) = I_0(t) + \frac{\epsilon_s}{a_\omega^2}\left|\tilde{f}(t/a_\omega)\tilde{\delta\phi}(t/a_\omega)\right|^2, \quad (14)$$

where ϵ_s is the absolute square of the integral over the unperturbed temporal field. This assumption is only true for a large enough ratio between the width of $\tilde{f}(t/a_\omega)\cdot\tilde{\delta\phi}(t/a_\omega)$ and $\tilde{E}_0(t)$. The accuracy of this approximation decreases with increasing beam size, since the width of the Fourier transform decreases with increasing beam size. Thus, we will systematically overestimate the spatial averaging and the amplitude of the perturbation term, when employing large beam sizes. We will provide an estimate of the uncertainty caused by this when discussing the beam sizes used in the experimental campaign.

If we now in a last step recognize how the Fourier transform of the height profile H of the surface is related to the PSD

$$\text{PSD} = \left|\tilde{H}(t/a_\omega)\right|^2 \Delta k, \quad (15)$$

with the spatial frequency spacing Δk, we can find a convenient formulation of the temporal profile using eq. 2

$$I(t) = I_0(t) + \frac{16\pi^2\epsilon_s}{a_\omega^2\lambda_0^2\Delta k}\left|\tilde{f}(t/a_\omega)\right|^2 \text{PSD}(t/a_\omega). \quad (16)$$

This formula enables us to predict the rising edge of a given experimental setup. It allows the calculation of the rising edge caused by optics in the near- and in the far-field for various beam sizes and shapes. While this work is concerned with the impact of the in-stretcher beam size on the temporal contrast, it is to note, that eq. 16 depends on the absolute square of the Fourier transform of the spatial profile at the considered optical element. If we consider a mirror in the near-field, the final formula depends on the spatial intensity distribution in the far-field and *vice versa*. Thus, the wavefront in the near-field directly influences the temporal contrast and aberrations of all kind can cause temporal contrast degradation. Therefore, it is crucial to control the wavefront in order to investigate the beam size dependence. We will later on use this insight to calculate an uncertainty

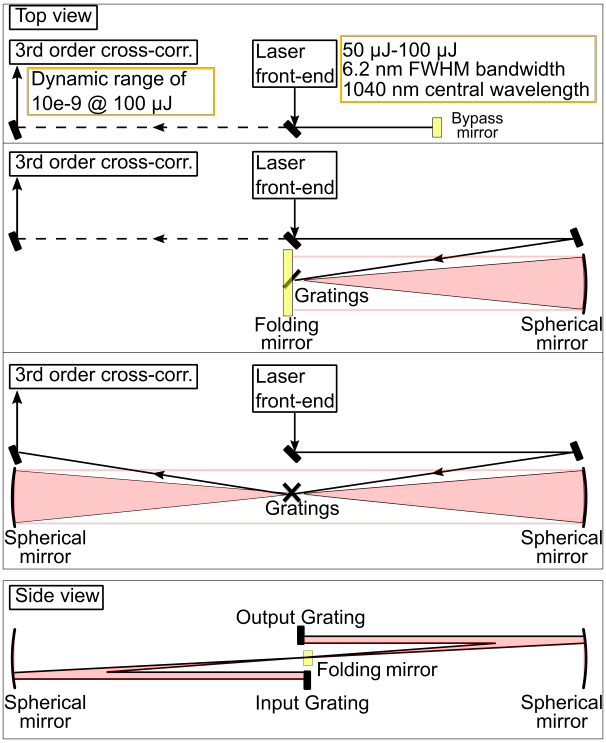

Figure 1: Schematic of the experimental stretcher setup with three configurations. First from top, the laser pulse bypasses the stretcher using the bypass mirror, second from top, the beam enters the stretcher, is incident on an optical grating (G) (g =1740$\frac{1}{\mathrm{mm}}$), and a spherical mirror ($R = 3.048\,\mathrm{mm}$), before being reflected from a folding mirror. And third from top, the pulse enters the stretcher and transverses through an unfolded design with two gratings and two spherical mirrors. In all three configurations the beam path ends in the third-order cross-correlator (Sequoia, Amplitude) with which the temporal profile is measured. The very bottom depicts a side view of the general setup.

for the temporal profile. It is further to note, that the PSD, which is originally a function of the spatial frequency of the surface is expressed here as a function over time. How this mapping can be done is covered in the appendix.

3. Experimental validation

In order to verify our findings, we built a test setup that included a temporally clean short pulse source, a variable stretcher in zero-stretch configuration and a scanning cross-correlator (Sequoia, Amplitude). The short pulses are produced by a commercial oscillator at a center wavelength of 1040 nm (Mira, Coherent), which are then further amplified by a homemade ultrafast optical parametric amplifier (uOPA) to several tens of microjoules and a full width half maximum (FWHM) bandwidth around 6.2 nm[11]. We were able to resolve the temporal profile of these pulses in the third-order cross-correlator over a dynamic range of nine orders of magnitude, which is sufficient for this analysis.

For the stretcher setup, we decided to use spherical mirrors for the telescope and a flat folding mirror that is positioned in the Fourier plane, as shown in Fig. 1. We positioned the gratings at half the radius of curvature too, in order to achieve a zero-stretch configuration. This way, we were able to measure the temporal profile directly after the stretcher without the need for a compressor. This allows us to isolate the influence of the telescope and the folding mirror.

The downside of this setup is that we can not investigate the impact of the stretcher gratings since the laser beam is not spectrally dispersed there, but we expect that the rising edge caused by gratings can be described analogously to mirrors. Thus, when investigating the spherical mirror and the folding mirror is sufficient in order to validate the analytical solution provided in this work, this solution allows us to predict the temporal profile for each optical element, even for the gratings. The described configuration would require us to stack two gratings on top of each other, which was cumbersome, thus we introduced a small mirror in the intermediate field between spherical mirror and grating. Since the spectral dispersion on this mirror is small we neglected its impact in the following considerations.

The stretcher, which is depicted in Fig. 1 can be either completely bypassed using a mirror on a magnetic mount or in two different configurations. The first of these two configurations is folded with a flat mirror located in the Fourier plane and the second is unfolded, ensuring that the beam size remains equal on all of its optics. All other parameters of the stretcher were kept constant for both configurations, especially the angle of incidence into the stretcher and the grating constant (and thus the spatial-dispersion coefficient a_ω).

During this experimental campaign, the temporal contrast was measured in all configurations for two different beam sizes. The results of those measurements are summarized in Fig. 2, where the background level of each measurement is given by the dynamic range of the cross-correlator. The top figure (a) depicts the measurements done in the folded design and the bottom figure (b) depicts the same measurements done in the unfolded configuration. Both configurations where used with a smaller beam size of $(1.1 \pm 0.05)\,\mathrm{mm}$, shown in blue and with a larger beam size of $(5.8 \pm 0.5)\,\mathrm{mm}$ shown in red. In order to emphasis the change of the slope of the rising edge that is caused by the change in beam size we included fits to the rising edge for the folded design. Those fits are expressed as black lines, with the steeper one corresponding to the smaller beam size (and thus larger focal spot). It is furthermore to note that the background level varies with the setup. This is due to the limited efficiency of the gratings which decreases the energy in the pulse and thus the intensity in the cross-correlator. For the larger beam size this is compensated for by a smaller focal spot in the cross-

correlator which leads to a higher intensity. The solution to the analytical approximation is also indicated in the figures, taking into account measurement uncertainties indicated as shaded areas. In order to calculate these solutions and later on their uncertainties, we had to measure several parameters. Firstly, the undisturbed temporal profile $I_0(t)$ was found using the Fourier transform of the spectrum, which is a valid approximation since the difference between the used laser pulse and its Fourier transform limit is negligible. Secondly, the spatial profile was obtained using a standard CCD-camera located in the near-field. This profile was then fitted by a Gaussian distribution, which gives the previously stated beam sizes.

But knowing the beam size in the near-field is not enough to assess the beam size in the far-field, where scattering from the folding mirror dominates. Thus, analytical Gaussian beam propagation and geometrical considerations of the impact of the diffraction from the grating onto the beam size and wavefront were used in order to estimate the actual beam sizes at the respective optical elements more accurately. For this we assumed the wavefront to be flat at the position of the CCD-camera (a fact that we will reconsider shorty, when we calculate the uncertainty of the calculated rising edge). The incorporation of the beam propagation over a distance of 2 m has a significant impact on the small beam size, but is almost negligible for the large beam size. Lastly, we estimated the PSD of the relevant optics, being the spherical mirror used for the telescope and the planar folding mirror. High spatial resolution data on the surface profile, was gathered at the metrology laboratory of CEA-CESTA, France, using a confocal microscope with a magnification between x0.5 and x1. The results of our PSD analysis are depicted in Fig. 3.

Now, for the calculation of the uncertainty of the rising edge we considered that the wavefront might not necessarily be flat at the position of the CCD-camera. We substituted the CCD-camera with a Shack-Hartmann-Sensor (SHS). Besides the estimation of the wavefront this was necessary because we had to align a magnifying telescope for the large beam and compensate diffraction for the small beam. The accuracy of the SHS, which consists of a mirco-lens array and a CCD-chip, is, without an absolute calibration, limited by the specifications of the mirco-lens pitch and the size of the CCD-chip (or more accurately, the mean distance between the pixels). Uncertainties in these two parameters directly translates to uncertainties in the defocus. We can estimate the uncertainty of the wavefront measured with the SHS to be a defocus of roughly $\pm 10^6 x^2$. This in turn contributes to the uncertainty of the beam size on the specific surfaces and thus the rising edge, that is indicated by the shaded areas in Fig 2. Another factor that contributes to this uncertainty is the fact that the beam size changes due to Gaussian beam propagation, especially for the small beam. This is included by comparing the results for the measured beam size at the stretcher input with the results that we find

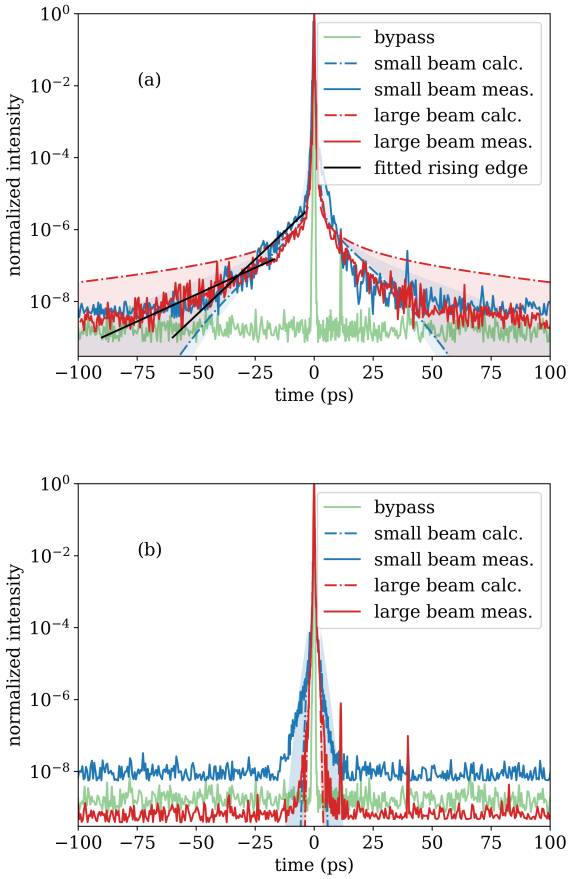

Figure 2: Measured temporal profile of a laser pulse that was amplified in a uOPA stage (bypass), after transversing through a folded stretcher (a) or an unfolded stretcher (b). The measurements were executed for a smaller beam size (FWHM=1.1 mm) and a larger beam size (FWHM=5.8 mm). Shaded areas indicate uncertainties of the alignment procedure. The black lines indicate the slope of the rising edge, with the steeper line corresponding to the smaller beam.

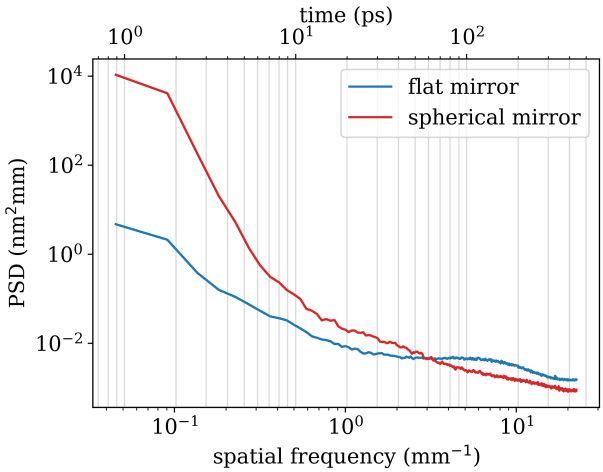

Figure 3: PSD of the spherical mirror and the flat folding mirror used in the stretcher setup, as common expressed in variance over frequency interval. Since the variance of the height distribution is approximately of the order of nm and the relevant spatial frequency interval of the order of mm^{-1}, we chose nm^{2}mm.

for the beam size that was calculated using Gaussian beam propagation. It is to note that the wavefront uncertainty improve the rising edge for all considered cases, since it increases the beam size on all surfaces. The uncertainty given by the Gaussian beam propagation on the other hand has a positive impact in the near-field, since it increases the near-field beam size, but a negative impact in the far-field, since it decreases the far-field beam size. While the defocus has some small impact on the rising edge caused by the spherical mirrors (Fig 2, (b)), its impact is more visible for the folded design (Fig 2, (a)). In this configuration the calculated defocus corresponds to an uncertainty in the waist location in the stretcher telescope of about one Rayleigh range, with respect to the setup. In other words, the uncertainty of the wavefront translates to an uncertainty of the beam size on the folding mirror of about a factor of two, which in turn can be understood as a change of the slope of the rising edge by a factor of two. We see that the contrast estimate given by a perfectly focused beam overestimates the contrast curve, while an increase of the beam size in the focus due to the slight defocus gives a better fit to the data. Another systematic error that has to be taken into account is the accuracy of the approximation that the Fourier transform of the spatial profile mapped onto the temporal domain is considerable wider than the FTL of the spectrum. For the small beam size the error caused by this approximation can be neglected, especially since the error would vanish in the otherwise calculated uncertainties. For the large beam size we can expect to underestimate the width of the smoothing function that is multiplied with the PSD by around 3%. At the same time we overestimate the amplitude of the term by also around 3%. All this shows that a good agreement between our experimental data and model exists, within the measurement uncertainty.

4. Discussion and conclusion

In this work, we showed how the beam size in the pulse stretcher can condition the rising edge of a laser pulse amplified by CPA. Our simple analytical model describes the interplay between beam size, PSD and temporal profile. This model confirms that the surface PSD of the optical elements is responsible for the rising edge but that its shape and slope is due to the beam size. In particular, the slope in the stretcher is steeper when the beam size is larger. Furthermore, we conducted an experimental campaign, during which we were able to push the point in time where the rising edge breaches the noise level (for the available energy in this proof-of-principle around 10^{-9}) from 55 ps to 5 ps, while using of-the-shelf optical components. The value of 55 ps was the best effort contrast for the folded design, which we found at the smallest tested beam size and thus largest focus. For the unfolded design, we observed a switch in the dependency on the beam size, as the roughness of the optical elements in the near-field prevails, yielding a better contrast for the larger beam. In this setup, the nine orders of magnitude contrast at 5 ps were achieved, which is a considerable improvement compared to the 55 ps that were possible in the folded setup.

When we compare this to the analytical solutions, we find a good agreement within the measurement uncertainty in the behavior of both, experiment and theory, as we can see that the folding mirror and the spherical mirror show an opposing dependency with the size of the beam that is incident in the stretcher. As it currently is this model is only valid for beams with an aspect ratio of around one, but it could be adapted to be applicable to elliptical beams by incorporating a second spatial integral into the considerations. A further limit of our analytical model that we find are the cases where, due to a large beam size, the rising edge is fully suppressed to times that are not considerably larger than the pulse length, since the approximation that allowed us to find eq. 13 is not valid in this region. The study of this region furthermore requires a measurement of the PSD over a larger sample size.

A consequence of this work is the necessity to develop new stretcher designs that do not incorporate optical elements in their Fourier plane, and at the same time it gives an analytical formulation that can be used to optimize PSD and beam size to reach a targeted contrast level. Such design rules can be derived from the interplay between rising edge and the aspect ratio on the surface, which is given by the in-stretcher beam size and the spatial-dispersion coefficient a_ω.

5. Appendix

The mapping of the PSD from spatial frequency to time can be done using the dependency between position and angular frequency of the spectrally-dispersed laser pulse in the stretcher $x_0 = a_\omega \omega$ and the numerical correspondence between x, k and t, ω:

$$dx = \frac{1}{dk(N-1)}, \quad dt = \frac{2\pi}{d\omega(M-1)} \tag{17}$$

Those two can be connected using the derivative of the mapping between position and angular frequency

$$\frac{dx}{d\omega} = a_\omega \tag{18}$$

Thus we find

$$\frac{1}{dk(N-1)} = dx = \frac{dx}{d\omega} d\omega = a_\omega d\omega = \frac{2\pi a_\omega}{dt(M-1)} \tag{19}$$

$$\Rightarrow dt = \frac{2\pi a_\omega dk(N-1)}{M-1} \tag{20}$$

as the step size of the time scale. Together with the length (M) this can be used to define the time array over which the PSD is known. Physically this means that each spatial frequency shifts energy to a specific time before and after the main peak by adding a spectral phase.

6. Acknowledgements

This work was carried out within the framework of the EUROfusion Consortium and received funding from the Euratom Research and Training Programme 2014–2018 and 2019–2020 under Grant Agreement No. 633053 (S.R. and V.B.). The views and opinions expressed herein do not necessarily reflect those of the European Commission.
The authors thank C. Rouyer, V. Beau and C. Leymarie from CEA-CESTA, France, for the access to their facility for the surface characterization of the optics used in this work.

References

1. D. Strickland and G. Mourou, Optics communications, **55**, 6 (1985).
2. J. Itatani, J. Faure, M. Nantel, G. Mourou, and S.Watanabe, Optics Communications, **148**, 1-3 (1998).
3. A. Jullien, O. Albert, F. Burgy, G. Hamoniaux, J.-P. Rousseau, J.-P. Chambaret, F. Aug´e-Rochereau, G. Ch´eriaux, J. Etchepare, N. Minkovski and S.M. Saltiel, Optics letters, **30**, 8 (2005).
4. R. C. Shah, R. P. Johnson, T. Shimada, K. A. Flippo, J. C. Fernandez, and B. M. Hegelich, High-temporal contrast using low-gain optical parametric amplification, Optics letters, **34**, 15 (2009).
5. L. Yu, Y. Xu, Y. Liu, Y. Li, S. Li, Z. Liu, W. Li, F. Wu, X. Yang, Y. Yang, C. Wang, X. Lu, R. Li and Z. Xu, Optics express, **26**, 3 (2018).
6. H. C. Kapteyn, M. M. Murnane, A. Szoke, and R. W. Falcone, Optics letters, **16**,7 (1991).
7. C. Ziener, P. Foster, E. Divall, C. Hooker, M. Hutchinson, A. Langley, and D. Neely, Journal of applied physics, **93**, 1 (2003).
8. D. Neely, C. Danson, R. Allott, F. Amiranoff, J. Collier, A. Dangor, C. Edwards, P. Flintoff, P. Hatton, M. Harman, M.-H.-R. Hutchinson, Z. Najmudin, D. A. Pepler, I. N. Ross, M. Salvati and T. Winstone, **17**, 2 (1999).
9. D. Hillier, C. Danson, S. Duffield, D. Egan, S. Elsmere, M. Girling, E. Harvey, N. Hopps, M. Norman, S. Parker, P. Treadwell, D. Winter and T. Bett , Applied Optics, **52**, 18 (2013).
10. C. Dorrer, I. Begishev, A. Okishev, and J. Zuegel, Optics letters, **32**, 15 (2007).
11. Y. Zobus, C. Brabetz, J. P. Zou, and V. Bagnoud in *Conference on Lasers and Electro-Optics (CLEO)*, STh2B.3 (2021).
12. L. Ranc, C. Le Blanc, N. Lebas, L. Martin, J. P. Zou, F. Mathieu, C. Radier, S. Ricaud, F. Druon, and D. Papadopoulos, Optics Letters, **45**, 16 (2020).
13. H. Kiriyama, M. Mori, A. S. Pirozhkov, K. Ogura, A. Sagisaka, A. Kon, T. Z. Esirkepov, Y. Hayashi, H. Kotaki, M. Kanasaki, H. Sakaki, Y. Fukuda, J. Koga, M. Nishiuchi, M. Kando, S. V. Bulanov, K. Kondo, P. R. Bolton, O. Slezak, D. Vojna, M. Sawicka-Chyla, V. Jambunathan, A. Lucianetti, and T. Mocek, IEEE Journal of Selected Topics in Quantum Electronics, **21**, 1 (2015).
14. R. P. Johnson, T. Shimada, and R. C. Shah, in *Laser Applications to Photonic Applications (CLEO)*, JWA44 (2011).
15. H. Donnelly and N. Ireland, "The Role of Near Time Coherent Contrast on Ultrafast Laser Driven Radiation Sources", Ph.D. thesis (Queen's University Belfast, 2021).
16. A. Dulat, C. Aparajit, A. Choudhary, A. D. Lad, Y. M. Ved, and G. R. Kumar, arXiv:2110.14595 (2021).
17. V. Bagnoud and F. Salin, JOSA B, **16**, 1 (1999).
18. C. Dorrer and J. Bromage, Optics Express, **16**, 5 (2008).
19. C. Hooker, Y. Tang, O. Chekhlov, J. Collier, E. Divall, K. Ertel, S. Hawkes, B. Parry, and P. Rajeev, Optics Express, **19**, 3 (2011).
20. J. Bromage, C. Dorrer, and R. Jungquist, JOSA B, **29**, 5 (2012).
21. J. Bromage, M. Millecchia, J. Bunkenburg, R. Jungquist, C. Dorrer, and J. Zuegel, in *Conference on Lasers and Electro-Optics (CLEO)*, CM4D.4 (2012).
22. V. A. Schanz, M. Roth, and V. Bagnoud, J. Opt. Soc. Am. A, **36**, 10 (2019).
23. X. Lu, X. Wang, Y. Leng, X. Guo, Y. Peng, Y. Li, Y. Xu,

R. Xu, and X. Qi, IEEE Journal of Selected Topics in Quantum Electronics, **24**, 5 (2018).
24. X. Lu, H. Zhang, J. Li, and Y. Leng, Opt. Lett., **46**, 21 (2021).